Classification: *Biological Sciences:* Biophysics

Detection of Bacteria in Suspension Using a Superconducting Quantum Interference Device

H. L. Grossman[*†], W. R. Myers[*†], V. J. Vreeland[†], R. Bruehl[†‡], M. D. Alper[†§], C. R. Bertozzi[†‡§¶], and John Clarke[*†]

Departments of [*]Physics, [‡]Chemistry, and [§]Molecular and Cell Biology, and [¶]Howard Hughes Medical Institute, University of California, Berkeley, CA 94720; [†]Materials Sciences Division, Lawrence Berkeley National Laboratory, Berkeley, CA 94720.

Corresponding author: John Clarke

Address: Department of Physics, 366 LeConte Hall #7300, University of California, Berkeley, CA 94720-7300

Telephone: 510-642-3069

Fax: 510-642-1304

Email: jclarke@socrates.berkeley.edu

Number of text pages and figures: 31

Number of words in abstract: 213

Total number of characters in paper: 46,395

Abbreviations: SQUID, superconducting quantum interference device; T_c, critical temperature

Abstract:

We demonstrate a technique for detecting magnetically-labeled *Listeria monocytogenes* and for measuring the binding rate between antibody-linked magnetic particles and bacteria. This assay, which is both sensitive and straightforward to perform, can quantify specific bacteria in a sample without the need to immobilize the bacteria or wash away unbound magnetic particles. In the measurement, we add 50 nm diameter superparamagnetic particles, coated with antibodies, to a liquid sample containing *L. monocytogenes*. We apply a pulsed magnetic field to align the magnetic dipole moments and use a high transition temperature Superconducting Quantum Interference Device (SQUID), an extremely sensitive detector of magnetic flux, to measure the magnetic relaxation signal when the field is turned off. Unbound particles randomize direction by Brownian rotation too quickly to be detected. In contrast, particles bound to *L. monocytogenes* are effectively immobilized and relax in about 1 s by rotation of the internal dipole moment. This Néel relaxation process is detected by the SQUID. The measurements indicate a detection limit of $(5.6 \pm 1.1) \times 10^6$ *L. monocytogenes* for a 20 μL sample volume. If the sample volume were reduced to 1 nL, we estimate that the detection limit could be improved to 230 ± 40 *L. monocytogenes* cells. Time-resolved measurements yield the binding rate between the particles and bacteria.

Introduction

Antibodies are widely used as biological probes to identify specific microorganisms or molecules (1, 2). The antibodies are linked to a label and introduced into the sample, where they bind to the targets of interest and provide a means of detection. Common labels include enzymes, fluorescent dyes, radioisotopes, or magnetic particles. This general technique has various applications. In an immunoassay, the goal is to detect and quantify specific targets. Tagged antibodies can also be used to separate target antigens selectively or to measure the affinity between antibody and antigen. In this paper, we present a sensitive method for detecting magnetically-labeled bacteria using a Superconducting Quantum Interference Device (SQUID), a highly sensitive detector of magnetic flux. This assay can be used to monitor bacteria in a liquid sample and to determine the rate of binding between antibody-linked particles and bacteria.

Magnetic particles have several advantages as labels. They are stable and nontoxic and can be manipulated with a magnetic field, making it possible to separate target antigens magnetically (3). In recent years, methods have been developed to detect small numbers of such particles using Hall probes (4), giant magnetoresistance arrays (5), atomic force microscopy (6), force amplified biological sensors (7), and SQUIDs (8-10).

Weitschies, Kötitz, and colleagues pioneered the use of SQUIDs for magnetic immunoassays (8, 11-16). They developed a magnetic relaxation immunoassay (MARIA) in which magnetic particles bound to targets are distinguished from unbound particles by their different relaxation times. Using a low critical temperature (T_c) SQUID, the group implemented a solid phase MARIA for detecting human immunoglobulin IgG. Enpuku *et al.* employed a high-T_c SQUID to detect human

interferon β (17). They labeled immobilized antigen with magnetic particles, applied a magnetic field to magnetize the particles, and measured the change in magnetic flux as the sample was passed under the SQUID.

In a previous communication (10), we described the use of a high-T_c SQUID microscope to detect immobilized targets, consisting of liposomes carrying the FLAG epitope, which were labeled with magnetic particles. Here, we demonstrate a method for detecting targets which are not immobilized, but rather are in suspension (Fig. 1). We couple 50 nm diameter γ-Fe_2O_3 particles to polyclonal antibodies raised against the bacterial pathogen *Listeria monocytogenes* and add them to a sample containing that organism. After allowing time for the particles to bind to the targets, we place the sample 130 μm above a high-T_c SQUID and apply a pulsed magnetic field to align the magnetic dipole moments. Each time the field is turned off, the SQUID detects the magnetic relaxation signal. Unbound particles relax in ~50 μs by Brownian rotation; this time is too short for the SQUID system to measure. Conversely, particles bound to the relatively large bacteria are able to rotate only slowly. These particles undergo Néel relaxation, in which their internal dipole moments relax to the lowest energy state. The resulting magnetic decay, which occurs over a time of roughly 1 s, is detected by the SQUID. Since the measured signal is due only to the bound particles, changes in the signal over time indicate the rate at which particles bind to bacteria.

Because this technique does not require immobilization of the targets or washing away of the unbound particles, it is straightforward to implement. It has the potential for improved accuracy over conventional immunoassays because there is no loss of materials during the process. We show that this technique can successfully differentiate between

bound and unbound particles and present results from titration experiments in which the concentration of either bacteria or particles is varied. We also show how the relaxation signal depends on the applied magnetic field, and we present time-resolved data demonstrating how this technique can be used to measure the rate of binding reactions. Finally, we discuss improvements to the technique and potential applications.

Theory

In this technique, we differentiate between bound and unbound particles by the different mechanisms by which they relax after the removal of a magnetic field. Brownian relaxation (18) is a physical rotation of the particles, with a relaxation time for a sphere

$$\tau_B = 3\eta V_H / k_B T , \qquad [1]$$

where η is the viscosity of the medium, V_H is the hydrodynamic volume, k_B is Boltzmann's constant, and T is the temperature. Taking T = 293 K and $\eta = 10^{-3}$ kg m^{-1} s^{-1}, we find $\tau_B \sim 50$ μs for particles with a hydrodynamic diameter of 50 nm.

Néel relaxation (19) originates from the anisotropy of the crystalline lattice. Many magnetic materials have an easy axis of magnetization such that when the crystal is magnetized along that axis, the energy is minimized. If an external field rotates the magnetization away from the easy axis, the magnetization will eventually return to its preferred direction upon removal of the field. The Néel relaxation time for a single domain particle is

$$\tau_N = \tau_0 \exp(KV_M / k_B T) , \qquad [2]$$

where $\tau_0 \sim 10^{-9}$ s, K is the magnetic anisotropy constant, and V_M is the volume of the magnetic core.

The particles used here were composed of γ-Fe_2O_3, for which the bulk anisotropy constant is $K \approx 2.5 \times 10^4$ J m^{-3}. The magnetic core of each particle consisted of a cluster of ~10 nm nanoparticles. While Eq. 2 predicts $\tau_N \sim 25$ ns for an individual 10 nm nanoparticle at T = 293 K, magnetic interactions between the nanoparticles within each core slow down the overall relaxation rate. Hence, the Néel relaxation time of these particles fell within the 1 ms to 1 s measurement window of our SQUID system.

Methods

SQUID Microscope. The measurement configuration is shown in Fig. 2. A direct current (dc) SQUID is a superconducting loop interrupted by two Josephson junctions, or weak links (20). When current-biased in the voltage state, the voltage oscillates quasi-sinusoidally as a function of the magnetic flux threading the SQUID loop with a period of the magnetic flux quantum, $\Phi_0 = h/2e \approx 2 \times 10^{-15}$ T m^2. To make the flux-to-voltage conversion linear, we operate the SQUID in a flux-locked loop that maintains the flux through it at a constant value; the output voltage of this feedback circuit is proportional to the flux applied to the SQUID. The SQUID used in these experiments was made from a 200 nm thick film of the high-T_c superconductor $YBa_2Cu_3O_{7-\delta}$ (YBCO) laser deposited onto a (100) $SrTiO_3$ bicrystal substrate and patterned by photolithography and argon ion milling. A bicrystal contains an in-plane misorientation of the crystallographic axis; an epitaxially grown film mimics the misorientation, forming a grain boundary which can support only a weak supercurrent. To form Josephson junctions, 2 μm wide microbridges

were patterned in the film across the grain boundary. The SQUID, shown in the inset of Fig. 3, had an effective flux capture area of 0.016 mm^2 and a peak-to-peak modulation amplitude of 11 μV. Operated with bias reversal (21), an electronic modulation scheme which reduces low frequency noise, it exhibited a white noise of 22 $\mu\Phi_0$ $Hz^{-1/2}$ at frequencies down to ~1 Hz.

The SQUID microscope (22) (Fig. 2) brings a biological sample at room temperature and atmospheric pressure very close to the SQUID, which is maintained at 77 K in a vacuum. Since the magnetic field from a collection of dipoles decreases with distance, it is important to minimize the separation between the sample and the SQUID. The SQUID was mounted on a sapphire rod thermally linked to a liquid nitrogen reservoir; these components were enclosed inside a fiberglass vacuum chamber. Above the SQUID, a 75 μm thick sapphire window separated the vacuum chamber from atmosphere. The gap between the SQUID and the window was 55 ± 10 μm, resulting in a total SQUID-sample distance of 130 ± 10 μm. The entire apparatus was enclosed in a triple layer μ-metal shield to attenuate the earth's magnetic field.

For each measurement, a sample holder was positioned on the window between two coils which provided a magnetizing field parallel to the plane of the SQUID. The sample holders consisted of 11 mm wide, 3.2 mm thick Lucite® squares. A 3.2 mm diameter hole was drilled through each square, and a 3 μm thick Mylar® film, attached to the Lucite with wax, sealed the bottom of the hole. The sample was offset laterally from the SQUID by 1.6 mm, one-half the sample diameter, thus maximizing the field from the sample which passed through the sensing area of the SQUID.

Bacteria. The target bacteria were the DP-L2161 strain (23) of *Listeria monocytogenes*, which has a deletion in the *hly* gene encoding listeriolysin O (LLO) and is thus 10^5 times less virulent than the wild-type strain (24). The *L. monocytogenes* were grown overnight in 3 mL of Brain Heart broth in an incubator-shaker (37 °C, 250 RPM). Prior to the assay, the bacteria were washed 3 times by centrifugation and resuspended in phosphate buffered saline. We counted the bacteria by measuring their optical density at 600 nm wavelength and multiplying it by 6×10^8 *L. monocytogenes*/mL to convert to concentration (25). Because the conversion factor depends on the phase to which the bacteria are grown, we estimate a counting error of ±20%. The K1 strain of *Escherichia coli* (26) was used as a control. The bacteria were grown overnight in 3 mL of Luria broth (Miller's LB broth) in an incubator-shaker (37 °C, 250 RPM), and washed and counted in the same manner as the *L. monocytogenes*. In this case, the optical density was multiplied by 1×10^9 *E. coli*/mL to convert to concentration (27).

Magnetic Particles. Superparamagnetic particles conjugated to monoclonal mouse anti-biotin antibodies were obtained from Miltenyi Biotec Inc. (Auburn, CA). The particles, composed of 55-59% γ-Fe_2O_3, 35-39% dextran, and 2-10% antibody by weight, were suspended in a buffer containing 0.05% sodium azide. Their hydrodynamic diameters ranged from 20-100 nm, with an average of 50 nm. The iron oxide core of each particle consisted of a cluster of ~10 nm nanoparticles.

Antibodies. The particles were coupled to polyclonal goat anti-*Listeria* IgG antibodies supplied by OEM Concepts (Toms River, NJ). The antibodies, raised against all

serogroups of *Listeria* species known to cause food-borne illness, were purified by the vendor on an antigen-affinity column with the *Listeria* bacteria immunogen preparation as antigen. The antibodies were biotinylated using the FluoReporter® Mini-Biotin-XX Protein Labeling Kit from Molecular Probes (Eugene, OR), which uses a 14-atom spacer. The protocol provided by Molecular Probes was modified to achieve approximately 1-3 biotin molecules per antibody.

Coupling of Antibodies to Particles. To couple the antibodies to the particles, we mixed the solution of biotinylated antibodies with the undiluted particle suspension, incubated the mixture overnight at 4 °C, and then filtered it through a 0.22 μm centrifugal filter with a low binding Durapore® PVDF microporous membrane (Millipore Corp., Billerica, MA) to eliminate particle aggregates. Ideally, we would have washed away the unbound antibodies, but we were unable to do this without a concomitant loss of particles. Instead, we varied the volume ratio of antibodies to particles to maximize the binding of the particles to *L. monocytogenes*. The binding signal increased progressively up to a ratio of 1.3:5, and thereafter remained constant up to 5.3:5. To ensure saturation of binding, a volume ratio of 4:5 was used for all subsequent particle preparations.

Results

Titration Experiments. To determine the sensitivity and specificity of the technique, we carried out a series of bacterial and particle titrations. The particle-antibody complexes and bacteria were prepared as described above and mixed together in various concentrations; the samples contained approximately 0.015% sodium azide. We

incubated the samples a minimum of 4 hours 45 minutes to ensure that at least 75% of the binding reaction would be complete at the time of the measurement. (The time required was determined from data discussed in the Binding Rate Measurements section.) Following the incubation period, each sample was agitated with a pipet to resuspend any material that had settled, and a sample holder containing 20 μL was placed on the microscope. We pulsed the 0.4 mT magnetic field on for 1 s and off for 1 s and recorded the magnetic decay each time the field was turned off. The data from 100 pulses were averaged. Observation of the samples under a phase contrast microscope indicated that the bacteria were nonmotile, and thus possibly dead, at the time of the measurement.

Typical time traces for an *L. monocytogenes* sample and associated controls are shown in Fig. 3. These data were fit to a sum of logarithmic and exponential functions. The logarithmic decay is characteristic of Néel relaxation for particles with a wide distribution of sizes, and therefore of relaxation times (28). We believe the exponential decay comes from particle aggregates, formed after the filtration step, which are large enough to Brownian relax on a measurable time scale without being bound to targets. The time constant for the exponential decay was typically ~15 ms, corresponding to a hydrodynamic diameter of ~340 nm for a sphere. The fitting function is

$$\Phi(t) = \Phi_{offset} + \Phi_s \ln(1 + \tau_{mag} / t) + \Phi_{\exp} \exp(-t / \tau_{\exp}) . \qquad [3]$$

Here, Φ_{offset} is an offset caused by the fact that the SQUID measures relative, rather than absolute, magnetic flux; Φ_s, the logarithmic decay amplitude, is proportional to the number of bound particles; τ_{mag} = 1 s is the magnetization time; Φ_{exp}, the exponential decay amplitude, depends on the number of unbound particle aggregates; and τ_{exp} = 15 ms is the exponential decay time.

The logarithmic decay amplitudes for the samples measured in the titration experiments are plotted in Fig. 4. For the bacterial titration, the concentration of *L. monocytogenes* or *E. coli* was varied, while the particle concentration was fixed at 0.05 relative to the stock suspension. For the particle titration, the particle concentration was varied, while the density of bacteria was fixed at 10^8/mL *L. monocytogenes* or *E. coli*.

There are several sources of error. SQUID noise, particularly at low frequencies, is the largest source of random error and was determined by fitting the individual traces to Eq. 3 and calculating the mean and standard deviation of the fit coefficients for 100 averages. The standard deviation, σ_s, of the logarithmic amplitude was typically ~10 $\mu\Phi_0$. We estimated other sources of error, such as variability among biological samples, by measuring a series of nominally identical samples. The standard deviation was found to be 6.9% of the signal level. Thus, the total error in Φ_s is

$$\sigma_{total} = \left[\sigma_s^2 + (0.069 \times \Phi_s)^2\right]^{1/2}, \qquad [4]$$

where the value of σ_s is determined separately for each sample measurement.

The logarithmic decay amplitude from the particles alone is very low (Fig. 4). It does not limit the sensitivity because when only a small number of targets are present, fewer particles are needed to saturate the binding sites. Therefore, if we find that a sample is dilute, we can reduce the magnitude of the background decay by using fewer particles.

The cross-reactivity to *E. coli* is also low (Fig. 4). The *E. coli* signal is only ~15% of the *L. monocytogenes* signal, assuming enough particles are present to saturate the *L. monocytogenes* binding sites. If we subtract out the control (particles alone) signal from the *L. monocytogenes* and *E. coli* data, the *E. coli* signal is less than 8% of the *L.*

monocytogenes signal. It could be reduced still further by adsorbing the antibodies against *E. coli* to eliminate cross-reactive groups.

The bacterial titration curve, shown in Fig. 4*A*, appears to have two distinct slopes, with a crossover at approximately 10^8 *L. monocytogenes*/mL. This shape may result from the polyclonal nature of the antibodies. We presume that there are various types of antibodies which are reactive against different epitopes and have different binding affinities. As each type of antibody is depleted, the slope of the curve decreases. Accordingly, we fit the data to a model in which there are two distinct types of antibodies, referred to as "A" and "B", and two corresponding types of antigenic determinants, also referred to as "A" and "B"; we chose this model for its simplicity, as well as for its consistency with the empirical observation of two nonzero slopes in Fig. 4*A*. The "A" and "B" in the model could represent two broad affinity classes of antibodies or two dominant antigenic determinants. We made the further assumption that each particle is conjugated exclusively to "A" or "B" antibodies. This assumption was based on data indicating that approximately 25% of the antibody-linked particles were reactive against this strain of *L. monocytogenes*[*]. Thus, the number of particles with more than one type of antibody against these bacteria should be relatively small.

[*] We carried out experiments in which we coupled biotinylated anti-*Listeria* antibodies to *L. monocytogenes* cells, washed away the unbound antibodies, and then added particles with anti-biotin on their surface. Measurements of the Néel relaxation signal yielded the magnetic signal per bacterium as well as the concentration of particles needed to saturate a given number of bacteria. In these experiments, we assumed that all the particles were capable of binding to *L. monocytogenes*. By comparing these results to those obtained in experiments in which the antibodies were linked to the particles at the outset, we determined that ~25% of the antibody-linked particles were reactive against *L. monocytogenes*.

The four independent parameters of the model are the fraction of "A" antibodies, the fraction of "A" antigens, the particle concentration required to saturate a given number of bacteria, and the magnetic signal produced by a saturated bacterium. Fitting simultaneously to the bacterial and particle titration curves, we varied the four parameters until chi-square

$$\chi^2 = \sum \left(\frac{\Phi_{s,measured} - \Phi_{s,calculated}}{\sigma_{total}} \right)^2 \qquad [5]$$

was minimized. The sum is taken over all data points. Here, $\Phi_{s,measured}$ is the measured logarithmic decay amplitude, $\Phi_{s,calculated}$ is the calculated amplitude with given fit parameters, and σ_{total} is the uncertainty in the measured amplitudes as determined by Eq. 4. The resulting fits are shown in Fig. 4. We find that the fraction of "A" antibodies is 0.53 ± 0.03; the fraction of "A" antigens is 0.99 ± 0.01; $(2.0 \pm 0.4) \times 10^9$ *L. monocytogenes*/mL are saturated by the full strength particle suspension; and each saturated *Listerium*/mL produces a $(3.6 \pm 0.7) \times 10^{-9}$ mΦ_0 logarithmic decay signal. The detection limit, taken as the minimum quantity of *L. monocytogenes* that can be detected with 95% confidence, is equal to twice the experimental uncertainty. Since $\sigma_{total} \approx \sigma_s$ in the limit of small Φ_s, the detection limit is $2\sigma_s \approx 20\ \mu\Phi_0$. This yields a sensitivity of $(5.6 \pm 1.1) \times 10^6$ *L. monocytogenes*/mL, corresponding to $(1.1 \pm 0.2) \times 10^5$ *L. monocytogenes* in a 20 μL sample volume.

Because the *L. monocytogenes* have so few "B" antigens, 0.0015 concentration particles are sufficient to saturate the "B" antigens in the particle titration shown in Fig. 4*B*. Hence, the slope change in this curve is barely visible.

Dependence of Signal on the Applied Magnetic Field. The alignment of the particle dipole moments increases with magnetic field until the field is strong enough to align them completely. To determine how the signal level depends on the applied field, we prepared a test sample to measure at various field strengths. We diluted the original particle suspension by a factor of 12.5, passed it through a 0.22 μm centrifugal filter, placed 20 μL in a sample holder, and allowed the liquid to evaporate. We measured the Néel relaxation signal of this sample in response to fields ranging from 0 to 2.2 mT, recording just one trace for each field value. Measurements were taken for both increasing and decreasing fields to ensure that there was no hysteresis. The results, plotted in Fig. 5, show that the signal can be increased by a factor of up to 3 by increasing the applied field above the 0.4 mT used in the titration experiments. (We did not use higher fields in the titration experiments because such fields require very precise alignment of the field coils, which is difficult to achieve. If the coils are not aligned sufficiently, then the applied field couples flux vortices into the SQUID, and excess SQUID noise results.)

Binding Rate Measurements. In another set of experiments, we measured the time dependence of the Néel relaxation signal. Because only bound particles contribute to the signal, the change in signal over time indicates the rate at which particles bind to bacteria. As in the titration experiments, we prepared the particle-antibody complexes, and washed and counted the bacteria. In quick succession, we mixed the particles and *L. monocytogenes*, vortexed the mixture for 5 s, and transferred 20 μL to a sample holder. We placed the sample on the SQUID microscope and measured the Néel relaxation signal

in response to a pulsed 0.4 mT field, taking 100 averages. The time between mixing the sample and obtaining the first measurement was 3-7 minutes. We repeated the measurement approximately every 4 minutes.

A typical dependence of SQUID signal on elapsed time is shown in Fig. 6, for 2.5×10^8 *L. monocytogenes*/mL and particles of concentration 0.05 relative to the stock suspension. The data were fit to an exponential function,

$$\Phi(t) = \Phi_{offset} + \Phi_{\exp}\left(1 - e^{-t/\tau}\right), \qquad [6]$$

where Φ_{offset} is the signal from particles that bind to bacteria during the mixing stage, the sum of Φ_{offset} and $\Phi_{\exp}$ is the equilibrium relaxation signal, and τ is the time constant for the post-mixing binding process. For the data in Fig. 6, $\Phi_{\text{offset}} = 0.045 \pm 0.005$ mΦ_0, $\Phi_{\exp} = 0.24 \pm 0.02$ mΦ_0, and $\tau = 209 \pm 39$ minutes. Approximately 16% of the total binding occurred during the initial mixing stage. The remainder of the binding took place over the course of many hours. The binding process may be diffusion-limited (29, 30).

Part of the increase in signal is due to settling of the bacteria and particles. The settling rate depends on the degree of cross-linking of the bacteria and particles – the larger the complexes formed, the faster the settling rate. To measure the settling rate, we prepared four different samples of bacteria and particles and allowed ample time for the binding to reach equilibrium (at least 24 hours at 4 °C). We then mixed each sample to resuspend any settled material, transferred 20 μL to a sample holder, and measured the time dependence of the signal. We found that the signals increased by 2.4% to 19%/hour, depending on the sample, corresponding to settling rates of 0.14 to 1.1 μm/s.

If we correct the data in Fig. 6 for settling using the largest observed settling rate and fit again to Eq. 6, we find the time constant for binding is lowered to 164 ± 31

minutes, a reduction of about 22%. Thus, the uncertainty in the settling rate contributes substantially to the uncertainty in the binding rate. The settling problem could be addressed by continuously mixing the sample during the course of the measurement. This would serve both to keep the targets in suspension and to speed up the binding process so that process-specific rates, rather than diffusion-limited rates, could be measured.

Discussion and Future Directions

The technique presented here has several possible applications. It could be implemented as an immunoassay to test for the presence of specific bacteria. Since it does not require immobilization of the targets or separation of the unbound tags, it could potentially provide more accurate quantification than conventional immunoassays. It could also be used to characterize the reactants in a system, as was done in fitting the titration data to the two antibody model. A distinctive feature of this technique is its ability to measure binding rates of reactants in suspension. The time series measurements could be expanded to determine how the binding rate depends on various experimental parameters. In addition, the technique could potentially be modified to measure bacterial transport, with applications in bioremediation. In order to implement bioremediation strategies successfully, one must be able to predict the transport of bacteria through contaminated media. However, most techniques for studying bacterial transport involve optical detection, making them ineffective for gauging movement through opaque media. By tagging the relevant bacteria with magnetic particles and using the SQUID to measure

changes in the magnetic signal over time, one could potentially study the movement of bacteria, through any type of medium, in real time.

As an immunoassay, this technique is specific, quantitative, reasonably fast, and moderately sensitive. The specificity depends largely on the antibodies used. For the affinity-purified anti-*Listeria* antibodies employed here, the cross-reactivity to *E. coli* was low – less than 8% of the *L. monocytogenes* signal, after correcting for background. The quantitative nature of the assay is evident from the titration data. We see in Fig. 4*A* that the signal increases linearly with bacterial concentration. The slope is constant so long as enough particles are present to saturate the *L. monocytogenes* binding sites. The speed of the assay is limited by the rate of binding of the particles to the bacteria. In these experiments, we incubated the samples several hours before performing measurements on them. However, by continuously mixing the samples during the binding process, one could expect to reduce the incubation time significantly. Further, in applications where high sensitivity or accuracy is not required, measurements could be taken before the binding reaction is complete.

The current detection limit is $(5.6 \pm 1.1) \times 10^6$ *L. monocytogenes*/mL, equivalent to $(1.1 \pm 0.2) \times 10^5$ *L. monocytogenes* in a 20 μL sample volume. The sensitivity to absolute number of bacteria could be greatly improved by decreasing the sample volume. For a sample much larger than the SQUID, as is currently the case, a sizeable fraction of the particles lie far away from the SQUID sensing area. Because the magnetic field from a dipole falls off as $1/\text{distance}^3$, these distant particles contribute little to the signal. By decreasing the sample volume, while holding the concentration of particles and targets fixed, one could increase the signal per particle, and hence improve the sensitivity.

For example, consider scaling down the sample volume to 1 nL by reducing the sample area to 0.01 mm^2 and the height to 0.1 mm. Since the SQUID effective area is 0.016 mm^2, the SQUID would capture the flux much more efficiently than in the current version. Further, because the new sample height would be comparable to the SQUID-sample separation, a particle at the top of the sample would contribute about 25% of the flux as one at the bottom. This contrasts sharply with the current configuration, in which particles at the top of the sample are so far away (2.7 mm) that their flux contribution is negligible. We calculate that a 1 nL sample of the above dimensions, located at its optimal position over the SQUID, would have a signal per particle 480 times greater than the current sample. Thus, the sensitivity of the technique would improve to 230 ± 40 *L. monocytogenes*. Note that while the sensitivity to number is highly dependent on sample volume, the sensitivity to concentration is relatively independent of sample volume.

A further sensitivity improvement could be achieved by immobilizing the bacteria on the Mylar base of the sample holder by means of a second antibody. This is essentially the method adopted in our earlier experiment (10) in which liposome targets were affixed to a Mylar film. In the current experiment, if we were to attach the bacteria in the 1 nL sample to the Mylar film, thereby bringing all the particles to within 130 μm of the SQUID, we calculate that the sensitivity would improve to 120 ± 20 bacteria. While immobilizing the targets requires an extra step, the return is greater sensitivity as well as the ability to detect a target of any size. Clearly, if an application requires detection of a small number of targets, it is highly desirable to immobilize the targets on a substrate or reduce the sample volume by concentration methods. Microfluidics could be

employed to implement a small volume assay, as well as to provide continuous mixing (31, 32).

We thank D. A. Portnoy for providing the *L. monocytogenes* culture and for helpful discussions, S.-K. Lee and H.-M. Cho for their help with the SQUID fabrication, T. M. Handel and colleagues for their assistance with the biological experiments, Y. R. Chemla for his early work on this assay, C. M. Klapperich and J. Song for technical assistance, and B. Dorval of OEM Concepts for providing the enzyme-linked immunosorbent assay (ELISA) protocol to test antibodies. This work was supported by the Director, Office of Energy Research, Office of Basic Energy Science, Materials Sciences and Engineering Division of the U.S. Department of Energy under Contract DE-AC03-76SF00098.

Figure legends

(1) Measurement procedure. A suspension of superparamagnetic particles, coupled to antibodies, is added to the liquid sample. (*A*) A magnetic field is applied to align the magnetic moments of the particles. (*B*) At time $t \sim \tau_B$ after the field is turned off, unbound particles have randomized direction by Brownian rotation, while particles bound to bacteria are still aligned. The magnetic moments of the bound particles will reorient slowly via Néel relaxation.

(2) Top portion of the SQUID microscope. The SQUID, inside a vacuum enclosure, is mounted on a sapphire rod thermally connected to a liquid nitrogen reservoir (not shown). A 75 μm thick sapphire window separates the vacuum chamber from atmosphere. The sample is contained in a Lucite holder, with a 3 μm thick Mylar base, aligned against a positioning element.

(3) Example of magnetic decay signals. For the traces shown, the concentration of bacteria was 10^8/mL, and the concentration of particles was 0.13 relative to the stock suspension. A 0.4 mT field was pulsed on for 1 s and off for 1 s, and data were recorded each time the field was turned off; 100 averages were taken. Since the particle-antibody complexes show little cross-reactivity to *E. coli*, the "*E. coli*" and "particles alone" curves overlay each other. Inset: Configuration of the YBCO SQUID. The slit is 4 μm wide.

(4) (*A*) Bacterial titration. The concentration of *L. monocytogenes* or *E. coli* was varied, while the particle concentration was fixed at 0.05 relative to the stock suspension. (*B*) Particle titration. The particle concentration was varied, while the bacterial concentration was fixed at 10^8/mL *L. monocytogenes* or *E. coli*. The magnetic relaxation signal of each sample was fit to a combination of logarithmic and exponential functions; the logarithmic amplitude of each sample is displayed. A two antibody model, described in the text, was used to fit the *L. monocytogenes* data.

(5) Dependence of the Néel relaxation signal on the applied magnetic field. The magnetic relaxation signal from a test sample, consisting of particles evaporated onto a sample holder, was measured for different values of applied field. Each decay curve was fit to a combination of logarithmic and exponential functions; the logarithmic amplitudes are shown.

(6) Binding rate measurement. *L. monocytogenes* (concentration 2.5×10^8/mL) and particle-antibody complexes (concentration 0.05 relative to the stock particle suspension) were mixed together, and the magnetic relaxation signal was measured as a function of time. Each decay curve was fit to a combination of logarithmic and exponential functions; the logarithmic amplitudes are shown. The amplitude versus time data were fit to $\Phi(t) = \Phi_{offset} + \Phi_{\exp}\left[1 - \exp(-t/\tau)\right]$. As a control, the signal from particle-antibody complexes alone (concentration 0.05 relative to the stock particle suspension) was measured over time.

References

1. Englebienne, P. (2000) *Immune and Receptor Assays in Theory and Practice* (CRC Press, Boca Raton).

2. Wild, D., ed. (2001) *The Immunoassay Handbook* (Nature Pub. Group, London).

3. Šafařík, I. & Šafaříková, M. (1999) *J. Chromatogr. B.* **722**, 33-53.

4. Besse, P.-A., Boero, G., Demierre, M., Pott, V., & Popovic, R. (2002) *Appl. Phys. Lett.* **80**, 4199-4201.

5. Miller, M. M., Sheehan, P. E., Edelstein, R. L., Tamanaha, C. R., Zhong, L., Bounnak, S., Whitman, L. J., & Colton, R. J. (2001) *J. Magn. Magn. Mater.* **225**, 138-144.

6. Baselt, D. R., Lee, G. U., Natesan, M., Metzger S. W., Sheehan, P. E., & Colton, R. J. (1998) *Biosens. Bioelectron.* **13**, 731-739.

7. Baselt, D. R., Lee, G. U., Hansen, K. M., Chrisey, L. A., & Colton, R. J. (1997) *Proc. IEEE* **85**, 672-680.

8. Weitschies, W., Kötitz, R., Bunte, T., & Trahms, L. (1997) *Pharm. Pharmacol. Lett.* **7**, 1-7.

9. Enpuku, K, Minotani, T., Gima, T., Kuroki, Y., Itoh, Y., Yamashita, M., Katakura, Y., & Kuhara, S. (1999) *Jpn. J. Appl. Phys.* **38**, L1102-L1105.

10. Chemla, Y. R., Grossman, H. L., Poon, Y., McDermott, R., Stevens, R., Alper, M. D., & Clarke, J. (2000) *Proc. Natl. Acad. Sci. USA* **97**, 14268-14272.

11. Kötitz, R., Matz, H., Trahms, L., Koch, H., Weitschies, W., Rheinlander, T., Semmler, W., & Bunte, T. (1997) *IEEE Trans. Appl. Superconductivity* **7,** 3678-3681.

12. Kötitz, R., Weitschies, W., Trahms, L., Brewer, W., & Semmler, W. (1999) *J. Magn. Magn. Mater.* **194**, 62-68.

13. Schambach, J., Warzemann, L., Weber, P., Kötitz, R., & Weitschies, W. (1999) *IEEE Trans. Appl. Superconductivity* **9**, 3527-3530.

14. Kötitz, R., Weitschies, W., Trahms, L., & Semmler, W. (1999) *J. Magn. Magn. Mater.* **201**, 102-104.

15. Haller, A., Hartwig, S., Matz, H., Lange, J., Rheinlander, T., Kötitz, R., Weitschies, W., & Trahms, L. (1999) *Supercond. Sci. Tech.* **12**, 956-958.

16. Lange, J., Kötitz, R., Haller, A., Trahms, L., Semmler, W., & Weitschies, W. (2002) *J. Magn. Magn. Mater.* **252**, 381-383.

17. Enpuku, K., Minotani, T., Hotta, M., & Nakahodo, A. (2001) *IEEE Trans. Appl. Superconductivity* **11**, 661-664.

18. Debye, P. (1929) *Polar Molecules* (Chemical Catalog, New York).

19. Néel, L. (1949) *Ann. Geophys.* **5**, 99-136.

20. Clarke, J. (1996) in *SQUID Sensors: Fundamentals, Fabrication and Applications,* ed. Weinstock, H. (Kluwer Academic, Dordrecht), pp. 1-62.

21. Koch, R. H., Clarke, J., Goubau, W. M., Martinis, J. M., Pegrum, C. M., & Van Harlingen, D. J. (1983) *J. Low Temp. Phys.* **51**, 207-224.

22. Lee, T. S., Dantsker, E., & Clarke, J. (1996) *Rev. Sci. Instrum.* **67**, 4208-4215.

23. Murray, E. G. D., Webb, R. A., & Swann, M. B. R. (1926) *J. Pathol. Bacteriol.* **29**, 407-439.

24. Jones, S. & Portnoy, D. A. (1994) *Infect. Immun.* **62**, 5608-5613.

25. D. A. Portnoy, personal communication.

26. Kauffmann, V. F. (1944) *Acta Pathol. Microbiol. Scand.* **21**, 20-45.

27. Elbing, K. & Brent, R. (2002) in *Current Protocols in Molecular Biology*, eds. Ausubel, F. M. *et al.* (John Wiley & Sons, New York), p. 1.2.2.

28. Berkov, D. V. & Kötitz, R. (1996) *J. Phys.: Condens. Matter* **8**, 1257-1266.

29. Rice, S. A. (1985) *Diffusion-Limited Reactions,* eds. Bamford, C. H., Tipper, C. F. H., & Compton, R. G. (Elsevier, New York).

30. Britton, N. F. (1986) *Reaction-Diffusion Equations and Their Applications to Biology* (Academic Press, Orlando).

31. Weigl, B. H., Bardell, R. L., & Cabrera, C. R. (2003) *Adv. Drug Deliver. Rev.* **55**, 349-377.

32. Chován, T. & Guttman, A. (2002) *Trends Biotechnol.* **20**, 116-122.

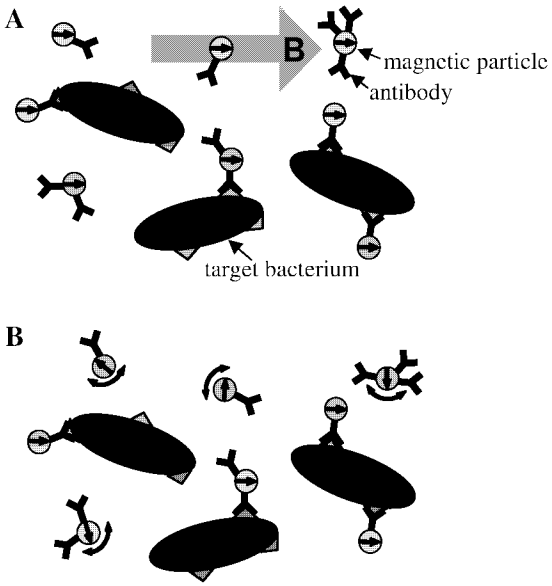

H. L. Grossman
Figure 1

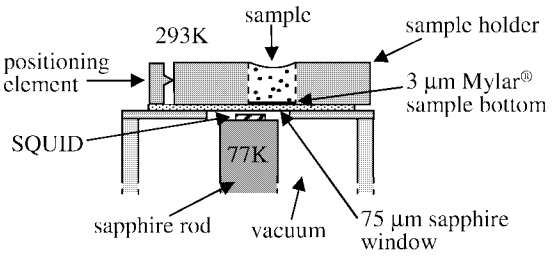

H. L. Grossman
Figure 2

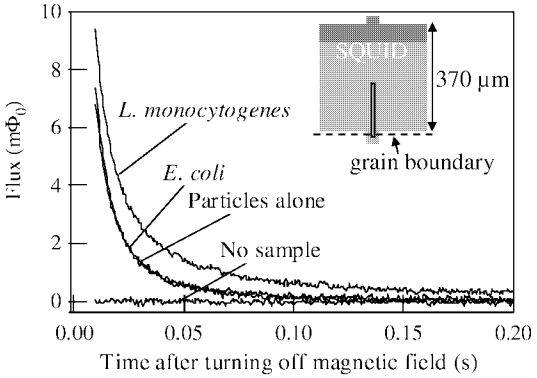

H. L. Grossman
Figure 3

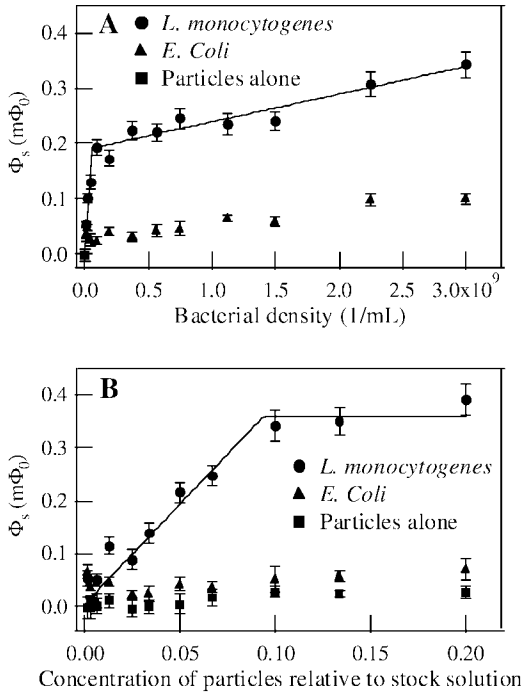

H. L. Grossman
Figure 4

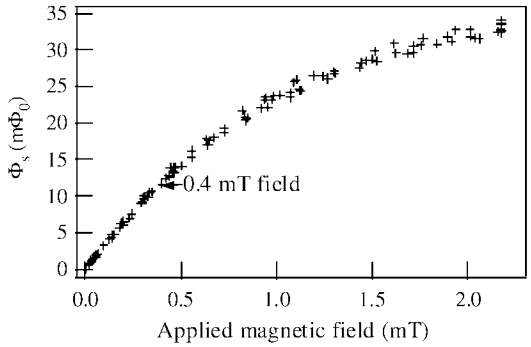

H. L. Grossman
Figure 5

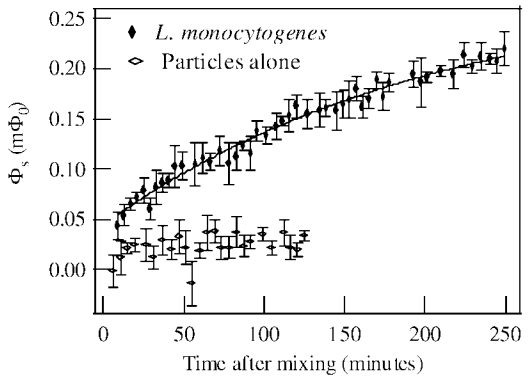

H. L. Grossman
Figure 6